World Academy of Science, Engineering and Technology
International Journal of Mechanical and Mechatronics Engineering
Vol:13, No:4, 2019

Sediment Patterns from Fluid-Bed Interactions: A Direct Numerical Simulations Study on Fluvial Turbulent Flows

Nadim Zgheib, Sivaramakrishnan Balachandar

***Abstract*—**We present results on the initial formation of ripples from an initially flattened erodible bed. We use direct numerical simulations (DNS) of turbulent open channel flow over a fixed sinusoidal bed coupled with hydrodynamic stability analysis. We use the direct forcing immersed boundary method to account for the presence of the sediment bed. The resolved flow provides the bed shear stress and consequently the sediment transport rate, which is needed in the stability analysis of the Exner equation. The approach is different from traditional linear stability analysis in the sense that the phase lag between the bed topology, and the sediment flux is obtained from the DNS. We ran 11 simulations at a fixed shear Reynolds number of 180, but for different sediment bed wavelengths. The analysis allows us to sweep a large range of physical and modelling parameters to predict their effects on linear growth. The Froude number appears to be the critical controlling parameter in the early linear development of ripples, in contrast with the dominant role of particle Reynolds number during the equilibrium stage.

***Keywords*—**Direct numerical simulation, immersed boundary method, sediment-bed interactions, turbulent multiphase flow, linear stability analysis.

I. Introduction

BEDFORMS are fascinating structures that result from the inherent instability of an erodible bed underlying a shearing flow field [1]. Bedforms may exist in aeolian and subaqueous environments and emerge under both laminar and turbulent flow fields. Their presence is of interest in a variety of disciplines. For example, the transport of water in pipes under certain conditions could result in bedform structures (usually in the form of ripples) that form within the pipes due to the presence of sand particles or other impurities in the water [2]. These structures represent an additional pressure drop, which may be significant compared to the losses caused by the smooth internal surface of the pipe. The interactions between bedforms and stationary obstacles are another example of great relevance to civil engineers. One of the main causes of failure of bridges is the scour problem [3]. This is a problem that is still heavily researched and not completely understood. Finally, the bedforms structures themselves could provide a great deal of detail about the overlying flow field that led to their formation. Indeed, many energy companies are interested in what is known as the inverse problem where the structure of the bedform is used to estimate the properties of the flow field (such as criticality, flow rate, flow depth, Reynolds number, etc.) responsible for its formation. Such properties could bear information on the carrying capacity of the flow (sediment size, density, and overall volume) and thus provide some detail on the nature and location of the deposit.

In short, bedforms are present in a variety of physical phenomena that are of great interest to a variety of scientific disciplines. It is only recently that advances in computational science have allowed specific features of these structures to be researched. Such features include the early evolution of bedforms from featureless erodible beds, the fluid-dynamical aspects behind the rich spectrum of bedform-bedform interactions, and the coupling between turbulence, sediment transport, and bed morphology for these complex structures. Many such features are very difficult if not practically impossible to capture experimentally.

The purpose of the present work is to analyse the early time evolution of ripples by conducting a hydrodynamic stability analysis on the Exner equation. The analysis is coupled with DNS of flow over a non-erodible wavy bed [4]-[7]. This approach is different from the classical hydrodynamic stability analysis in the sense that the DNS naturally provide the phase shift between the bed shear stress and the bed topology. The empirical relationship in [8] is then used to extract the sediment flux from the bed shear stress, and with it the phase lag between the sediment flux and the bed topology. Once the phase lag is known, each simulation can be used to test for the effects of a variety of parameters on the wavelength of the developing ripples.

II. Direct Numerical Simulations

A. Mathematical Model

We solve the conservation of mass and momentum equations in a rectangular domain as shown in Fig. 1.

$$\nabla \cdot \boldsymbol{u} = 0\,, \tag{1}$$

$$D\boldsymbol{u}/Dt = \boldsymbol{e}_x - \nabla p + Re_\tau \nabla^2 \boldsymbol{u}/Re_\tau + \boldsymbol{f}. \tag{2}$$

In (1) and (2), $\boldsymbol{u}$ represents the three components of the velocity field. $\boldsymbol{e}_x$ is a unit vector in the x-direction and here represents the non-dimensional mean pressure gradient. p corresponds to the perturbation pressure due to turbulent

N. Zgheib is with the School of Engineering, Lebanese American University, Byblos, Lebanon (phone: +961 9 547 254; fax: +961 9 546 008; e-mail: nadim.zgheib@lau.edu.lb).

S. Balachandar is with the Mechanical & Aerospace Engineering Department, University of Florida, Gainesville, FL 32601 USA (e-mail: bala1s@ufl.edu).

fluctuations, $\boldsymbol{f}$ is the coupling force that is imposed on the immersed boundary to ensure the no-slip and no-penetration conditions are satisfied at the bed, and Re_τ is the shear Reynolds number defined using the velocity and length scales as

$$Re_\tau = U_\tau^* H_f^* / \nu^*. \tag{3}$$

Here, H_f^* corresponds to the mean flow depth, ν^* is the kinematic viscosity of the fluid, and U_τ^* is the average shear velocity on the bed. Throughout the manuscript, the asterisk denotes a dimensional quantity, while all other parameters are to be treated as non-dimensional with respect to the aforementioned scales.

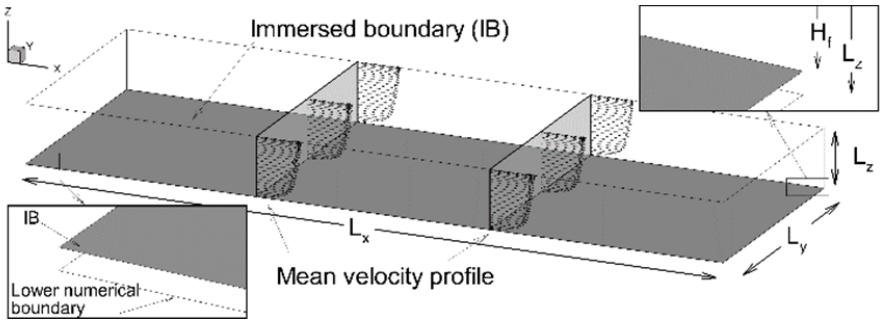

Fig. 1 Rectangular numerical domain with a flat sediment bed accounted for by the immersed boundary. $L_x = 4$, $L_y = 12$, $L_z = 1.005$, $H_f = 1$

A total of 11 simulations were performed, the details of which are shown in Table I. The present resolution of $288 \times 96 \times 301$ grid points along the streamwise, spanwise, and vertical directions was chosen to match recent studies [10], [11] for $Re_\tau = 180$.

TABLE I
LIST OF SIMULATIONS. λ AND δ ARE THE WAVELENGTH AND AMPLITUDE OF THE SINUSOIDAL DISTURBANCE OF THE BED

Simulation number	λ	δ
S0	∞	0
S1	$L_x/1$	2×10^{-3}
S2	$L_x/2$	2×10^{-3}
S3	$L_x/3$	2×10^{-3}
S4	$L_x/4$	2×10^{-3}
S6	$L_x/6$	2×10^{-3}
S8	$L_x/8$	2×10^{-3}
S10	$L_x/10$	2×10^{-3}
S12	$L_x/12$	2×10^{-3}
S14	$L_x/14$	2×10^{-3}
S16	$L_x/16$	2×10^{-3}

B. Hydrodynamic Stability Analysis

We perform a linear stability analysis with a small, spanwise invariant, sinusoidal disturbance to an otherwise flat, non-erodible bed using the Exner equation

$$\varphi \, \partial\eta/\partial t = -\nabla \cdot \boldsymbol{q} + \varepsilon \langle |\boldsymbol{q}| \rangle \nabla^2 \eta. \tag{4}$$

Here, η represents the sediment bed elevation and $\boldsymbol{q}$ the sediment flux vector. φ is the volume fraction and is assigned a constant value of $\varphi = 0.6$, and $\varepsilon = 4$ is an adjustable parameter [9] that controls the numerical diffusion term.

Since the stability analysis is spanwise invariant, we only need to consider a simplified form of the Exner equation with no spanwise dependence, i.e. the 1-D Exner equation.

$$\varphi \, \partial\eta/\partial t + \partial\bar{q}/\partial x = \varepsilon \bar{\bar{q}} \partial^2 \eta / \partial x^2. \tag{5}$$

$\bar{q}$ is the bedload volumetric flux of particles and $\bar{\bar{q}}$ is the mean bedload flux over the entire bed. These quantities are computed using the bed shear stress of the three-dimensional simulations presented in Table I as follows. Once the flow reaches a stationary state, it is span and time averaged to yield the corresponding span and time averaged bed shear stress $\langle \overline{\tau^*} \rangle(x)$. $\langle \overline{\tau^*} \rangle(x)$ is then used to compute the average Shields number $\langle \overline{\Theta} \rangle(x)$, which in turn is needed to compute $\bar{q}(x)$ and $\bar{\bar{q}}$. More specifically, as indicated in Table II, which defines some of the variables used in this study as well as notation and nomenclature, the span and time averaged quantities are expressed as

$$\langle \overline{\Theta} \rangle = \langle \overline{\tau^*} \rangle / \left[\left(\rho_p^* - \rho_f^* \right) g^* d_p^* \right] \tag{6}$$

$$\bar{q} = \left(Re_p / Re_\tau \right) c_1 (\langle \overline{\Theta} \rangle - \Theta_{cr})^{c_2} \tag{7}$$

$$\bar{\bar{q}} = \left(Re_p / Re_\tau \right) c_1 \left(\langle \overline{\overline{\Theta}} \rangle - \Theta_{cr} \right)^{c_2}. \tag{8}$$

where c_1 and c_2 are parameters of the bedload transport model.

The modified Exner equation in (5) is the only expression needed to carry out the stability analysis. The simulations serve to provide the input to (5) in the form of $\overline{\Theta}$, from which $\bar{q}$ and $\bar{\bar{q}}$ are computed. This constitutes the main difference between the present analysis and previous studies in which the bedload flux is modelled by assuming a phase shift with respect to the bed elevation.

The stability analysis consists of first Fourier expanding $\eta(x,t)$ and $\langle \overline{\Theta} \rangle(x,t)$ up to the first order terms

$$\eta = \eta_0 + \eta_1 e^{\alpha_1 t} e^{\mathbf{i} \frac{2\pi x}{\lambda}} + complex\ conjugate \tag{9}$$

$$\langle \overline{\Theta} \rangle = \langle \overline{\Theta} \rangle_0 + \langle \overline{\Theta} \rangle_1 e^{\alpha_1 t} e^{\mathbf{i} \frac{2\pi x}{\lambda}} + complex\ conjugate \tag{10}$$

In the above, $\eta_0 = 0$ is the mean bed elevation, and $\langle\overline{\Theta}\rangle_0 = \langle\overline{\overline{\Theta}}\rangle$. The coefficients η_1, $\langle\overline{\Theta}\rangle_1$, and α_1 are complex

$$\eta_1 = \eta_{1R} + i\eta_{1I} \tag{11}$$

$$\langle\overline{\Theta}\rangle_1 = \langle\overline{\Theta}\rangle_{1R} + i\langle\overline{\Theta}\rangle_{1I} \tag{12}$$

$$\alpha_1 = \alpha_{1R} + i\alpha_{1I} \tag{13}$$

However, since the prescribed sinusoidal disturbance is of the form $\eta = \delta\cos(2\pi x/\lambda)$ as shown in Fig. 2, it follows that η_{1I} is identically zero and $\eta_{1R} = \delta$. As for the Shields number $\langle\overline{\Theta}\rangle_1$, we note that the presence of a non-zero imaginary component indicates a phase shift between the shear stress and the bed topology. We know from the previous studies [12] that such a phase shift is necessary for the bed to be unstable. Finally, the exponential time coefficients, α_{1R} and α_{1I} represent the growth rate and phase speed of the bedform, respectively.

TABLE II
SYMBOLS, NOTATION, AND NOMENCLATURE DEFINITION. (* DENOTES DIMENSIONAL QUANTITY)

Variable/Notation	Symbol	Mathematical expression
Particle diameter	d_p^*	-
Particle density	ρ_p^*	-
Fluid density	ρ_f^*	-
Submerged specific gravity	R	$(\rho_p^* - \rho_f^*)/\rho_f^*$
Gravitational acceleration	g^*	-
Particle Reynolds number	Re_p	$\frac{1}{\nu^*}\sqrt{Rg^*d_p^{*3}}$
Shear Reynolds number	Re_τ	$U_\tau^* H_f^*/\nu^*$
Froude number	Fr_τ	$U_\tau^*/\sqrt{g^* H_f^*}$
Bed-normal velocity gradient	$\partial u/\partial n$	-
Bed shear stress	τ^*	$\left(\frac{\mu^* U_\tau^*}{H_f^*}\right)\frac{\partial u}{\partial n}$
Shields number	Θ	$\tau^*/\left[(\rho_p^* - \rho_f^*)g^* d_p^*\right]$
Critical Shields number	Θ_{cr}	$\frac{1}{2}\left[0.22\, Re_p^{-0.6} + 0.06\, exp\left(-17.77\, Re_p^{-0.6}\right)\right]$
Volumetric flux per unit width	q	$q = \left(Re_p/Re_\tau\right) c_1(\Theta - \Theta_{cr})^{c_2}$
Time average of quantity ■	$\langle\blacksquare\rangle$	$\frac{1}{T}\int_{t_1}^{t_1+T} \blacksquare\, dt$
Spanwise average of quantity ■	$\overline{\blacksquare}$	$\frac{1}{L_y}\int_0^{L_y} \blacksquare\, dy$
Stream and span average of quantity ■	$\overline{\overline{\blacksquare}}$	$\frac{1}{L_x L_y}\int_0^{L_y}\int_0^{L_x} \blacksquare\, dxdy$
Real and imaginary components of complex quantity ■	$\blacksquare_R$ & $\blacksquare_I$	-

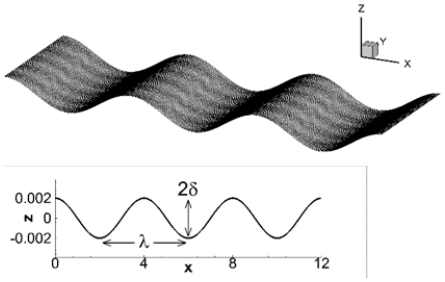

Fig. 2 Shape of sinusoidal sediment bed (i.e. immersed boundary)

One of the main objectives of the linear stability analysis is to find the growth rate of the most amplified mode. That is, we are interested in identifying the wavelength λ in Fig. 2, for which α_{1R} is a maximum. From the above equations, we can compute the growth rate α_{1R} as

$$\alpha_{1R} = \left[\left(Re_p/Re_\tau\right) c_1\left(\langle\overline{\overline{\Theta}}\rangle - \Theta_{cr}\right)^{c_2-1}\right](2\pi/\lambda\varphi)\left[c_2(\langle\overline{\Theta}\rangle_{1I}/h_{1R}) - \varepsilon(\langle\overline{\overline{\Theta}}\rangle - \Theta_{cr})(2\pi/\lambda)\right] \tag{14}$$

While the temporally-evolving simulations presented in [10] were useful in dissecting the various stages of evolution observed in the experiments of [13], the simulations are only representative of the specific set of conditions used therein. In the present study, we test the applicability of hydrodynamic stability analysis in predicting the initial evolution of an erodible bed with the advantage that the same simulation could be used to predict the initial stages of bedform evolution for a wide range of parameters. On the other hand, the stability analysis is only useful for the early linear stages of bed evolution unlike the erodible bed simulations in which the bed and the flow can interact non-linearly and evolve continuously in a complex manner.

In Fig. 3, we show a plot of the growth rate versus wavelength for two cases with parameters corresponding to two simulations from [10]. Both cases have the same particle Reynolds number $Re_p = 4.34$, but different Froude numbers $Fr_\tau = 0.032$ (panel (a)) and $Fr_\tau = 0.019$ (panel (b)). The dashed vertical line marks the value of the wavelength λ for which α_{1R} attains its maximum value, i.e. the most amplified mode. This wavelength, which we will term λ_{max} is likely to be the wavelength of the early bedforms observed under these flow and bed conditions. In fact, we find the values of λ_{max} for the cases in Fig. 3 and those observed in [10] to be in good agreement with one another as shown in Table III.

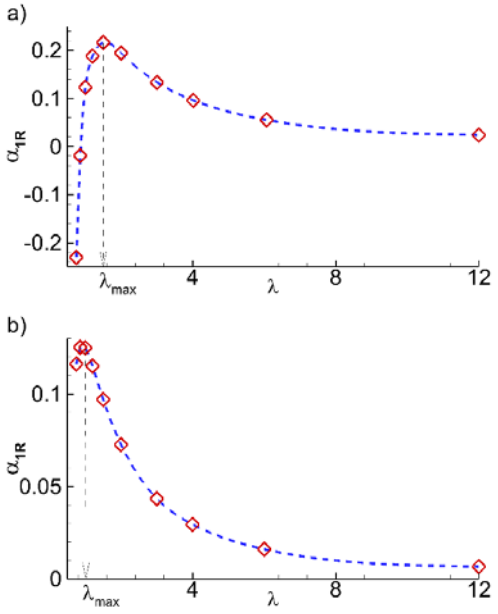

Fig. 3 Growth rate α_{1R} versus wavelength λ obtained from the simulations in Table I for a) $Fr_\tau = 0.032$ & $Re_p = 4.34$ and b) $Fr_\tau = 0.019$ & $Re_p = 4.34$

TABLE III
MOST AMPLIFIED WAVELENGTH FROM PRESENT ANALYSIS AND [10]. THE TWO BOLDED ROWS CORRESPOND TO THE CASES IN FIG. 3

Fr_τ	Re_p	λ_{max} from [10]	λ_{max} (present stability analysis)
$\mathbf{3.27 \times 10^{-2}}$	$\mathbf{4.34}$	$\mathbf{\sim 1.4}$	$\mathbf{\sim 1.5}$
$\mathbf{1.92 \times 10^{-2}}$	$\mathbf{4.34}$	$\mathbf{\sim 1.2}$	$\mathbf{\sim 0.93}$
3.27×10^{-2}	0.84	~ 1.4	~ 1.5

The plots in Fig. 3 and the corresponding data in Table III are valid for a specific set of flow and particle parameters, namely those used in the simulations of [10]. In the case of DNS of a temporally and spatially evolving bed, new simulations would be required to investigate different flow and particle parameters, or implement a different model for sediment transport. On the other hand, with the present approach of linear stability analysis, provided Re_τ remains unchanged, no new simulations are required to sweep the particle parameters or to test different sediment transport models. We can thus isolate the effects of each of the parameters in. (14).

We varied all the parameters in (14) over a wide range of values. We observed the Froude number to be the controlling parameter for initial bedform development. On the other hand, the role of all the other parameters considered was found to be less critical when compared to the Froude number. This is in contrast with the dominant role of the particle Reynolds number during the equilibrium stage of bedforms, at least in the case of ripples.

ACKNOWLEDGMENT

This study was supported by ExxonMobil Upstream Research Company through grant EM09296.

REFERENCES

[1] Kennedy, J. F. (1969). The formation of sediment ripples, dunes, and antidunes. *Annual Review of Fluid Mechanics*, *1*(1), 147-168.
[2] Elliot, A. H., & Brooks, N. H. (1997). Transfer of nonsorbing solutes to a streambed with bed forms: Laboratory experiments. *Water Resour. Res*, *33*(1), 137-151.
[3] Breusers, H. N. C., Nicollet, G., & Shen, H. W. (1977). Local scour around cylindrical piers. *Journal of Hydraulic Research*, *15*(3), 211-252.
[4] Zilker, D. P., Cook, G. W., & Hanratty, T. J. (1977). Influence of the amplitude of a solid wavy wall on a turbulent flow. Part 1. Non-separated flows. *Journal of Fluid Mechanics*, *82*(1), 29-51.
[5] Hudson, J. D., Dykhno, L., & Hanratty, T. J. (1996). Turbulence production in flow over a wavy wall. *Experiments in Fluids*, *20*(4), 257-265.
[6] Cherukat, P., Na, Y., Hanratty, T. J., & McLaughlin, J. B. (1998). Direct numerical simulation of a fully developed turbulent flow over a wavy wall. *Theoretical and computational fluid dynamics*, *11*(2), 109-134.
[7] Calhoun, R. J., & Street, R. L. (2001). Turbulent flow over a wavy surface: Neutral case. *Journal of Geophysical Research: Oceans*, *106*(C5), 9277-9293.
[8] Meyer-Peter, E., & Müller, R. (1948). Formulas for bed-load transport. In *IAHSR 2nd meeting, Stockholm, appendix 2*. IAHR.
[9] Cayocca, F. (2001). Long-term morphological modeling of a tidal inlet: the Arcachon Basin, France. *Coastal Engineering*, *42*(2), 115-142.
[10] Zgheib, N., Fedele, J. J., Hoyal, D. C. J. D., Perillo, M. M., & Balachandar, S. (2018a). Direct numerical simulation of transverse ripples: 1. Pattern initiation and bedform interactions. *Journal of Geophysical Research: Earth Surface*.
[11] Zgheib, N., Fedele, J. J., Hoyal, D. C. J. D., Perillo, M. M., & Balachandar, S. (2018b). Direct Numerical Simulation of Transverse Ripples: 2. Self-Similarity, Bedform Coarsening, and Effect of Neighboring Structures. *Journal of Geophysical Research: Earth Surface*.
[12] Bennett, S. J., & Best, J. L. (1995). Mean flow and turbulence structure over fixed, two-dimensional dunes: implications for sediment transport and bedform stability. *Sedimentology*, *42*(3), 491-513.
[13] Coleman, S. E., & Melville, B. W. (1996). Initiation of bed forms on a flat sand bed. *Journal of Hydraulic Engineering*, *122*(6), 301-310.